A simplified detection efficiency calibration method using point source model in Tomographic Gamma Scanning

HAN Miaomiao[1], GUO Zhirong[1, 2], PENG Minjun[1], LIU Haifeng[2], LI Qinghua[2], and CHEN Xianglei[2]

1. Fundamental Science on Nuclear Safety and Simulation Technology Laboratory, Harbin Engineering University, Harbin 150001, China (miaomiaohan321@163.com; heupmj@163.com)

2. Wuhan Second Ship Design and Research Institute, Wuhan 430205, China (guoeg112@sina.com; liuhf2634@163.com; liqinghua@whhwtech.com; chenxianglei@whhwtech.com)

Abstract: Detection

As the precondition of Tomographic Gamma Scanning (TGS) technique to assay nuclear waste drums, detection efficiency calibration is an essential task and needs high accuracy for the emission reconstruction stage. As a key issue, how to conduct detection efficiency calibration for the TGS technique still needs to be solved, without by means of the existing commercial detection efficiency calibration software such as the In Situ Object Counting System/Software (ISOCS). In this paper, TGS measurement geometries are analyzed using the point source model in detail from three aspects, *i.e.*, limited fields of view (FOVs) of the collimated High Purity Germanium (HPGe) detector, the spatial position overlap and the symmetry of point sources relative to the collimated HPGe detector, intending to obtain independent matrix elements in the calibrated detection efficiency matrix to avoid redundant workload. Then, the Monte Carlo N-Particle (MCNP) code as a Monte Carlo simulation method is used to compute values of these independent detection efficiency matrix elements. To verify detection efficiency calibration results, two different 200 liters drums are simulated with the same 3 gamma point sources distribution of different inner-heights and radio-activities. Algebraic Reconstruction Technique (ART) with the non-negativity constraint and Maximum Likelihood Expectation Maximization (MLEM) are respectively applied to the emission reconstruction stage. Results reveal that all 3 point sources can be easily recognized and precisely located, and their own corresponding radio-activities fit standard setting values very well with relative errors ~ 3%, indicating the feasibility of the simplified method to calibrate detection efficiency using point source model in TGS technique.

Keyword: Tomographic Gamma Scanning (TGS); radioactive waste drums; detection efficiency calibration; point source model

1 Introduction

Tomographic Gamma Scanning (TGS) is a technique developed by Estep *et al*. [1] to characterize gamma radio-nuclidic composition of nuclear waste drums for national regulations of nuclear waste disposition, transportation, temporary and permanent storage. If there are attenuation materials which are regularly called attenuation matrices in nuclear waste drums, γ-rays from radioactive sources inside drums will be attenuated when reach the detector. In order to locate these gamma radioactive sources and obtain their radio-activities, the TGS technique is divided into two stages, *i.e.*, the transmission reconstruction stage, and the emission reconstruction stage. The former stage provides linear attenuation coefficients of all voxels inside the drum for the attenuation correction of the latter stage. But before attenuation correction in the latter stage, the un-attenuated three-dimensional (3D) detection efficiency distribution of all gamma radioactive sources inside drums must have been done in advance. So far, Canberra Industries Inc. develops a mathematical efficiency calibration software - In-Situ Object Calibration Software (ISOCS) using a combination of Monte Carlo, numerical integration, and ray-tracing methods[2, 3]. In ISOCS theory, an accurate MCNP (Monte Carlo N-Particle) model of a specific radiation detector is firstly created and then validated by comparisons to a series of carefully controlled comparisons to NIST (National Institute of Standards and Technology)-traceable reference point sources to adjust parameters of the MCNP model so

Received date: July 13, 2018
(Revised date: September 9, 2018)

that the measured efficiency matches the MCNP modeled efficiency at ~10 energies and multiple spatial locations. This validated MCNP detector model is then used to compute the efficiency at about 800 different locations at multiple distances and many locations. These point-efficiencies are then integrated into a spatial map and supplied as a detector characterization file with that specific detector. In TGS model of this paper, the number of detection efficiencies needed to calibrate is about 10^7, which also shows that there are still a variety of point sources needed to computed at different energies with the detector used. A simplified method to calibrate detection efficiency is proposed in this paper to greatly reduce the number of point sources that are needed to be calibrated. This method can not only be used in TGS technique but also can be used in the existing commercial ISOCS software to simplify the process of detection efficiency calibration without considering the limited types of specific detectors validated yet. In this paper, different measurement geometries of TGS instrument are analyzed in detail to obtain independent matrix elements in the calibrated detection efficiency matrix to avoid redundant workload. Measurements of two different 200 liters drums are simulated by the MCNP[4] code to verify obtained detection efficiency calibration results.

2 Theory

2.1 TGS configuration

In this paper, the TGS technique is used to assay national standard 200 liters drum, with the interior height of 85.0 cm, the interior diameter of 56.0 cm. The drum is averagely partitioned into 16 layers and each layer is averagely subdivided into 100 sections according to 2 perpendicular diameters of the drum displayed in Fig. 1. The part outside each layer of the drum is truncated to obtain 88 voxels, which are composed of 60 voxels of the same regular cubic shape and 28 voxels of different irregular shapes [5] displayed in Fig. 1. Based on the assumption that each voxel is filled with uniform matrices and the point source model that gamma radioactive sources in each voxel is thought as a point source located in the centroid position of each regular and irregular voxel, there are 16*88 = 1,408 voxels and point sources inside the whole drum displayed in Fig. 2.

A high-resolution p-type coaxial HPGe detector is used with the relative efficiency of 30% displayed in Figs. 1 and 2. The collimator of the HPGe detector is of a truncated diamond-shaped window and its size is slightly larger than the end cap of the HPGe detector displayed in Fig. 3. Compared with the end cap of HPGe detector, the reason why the collimator window is especially designed like this lies in that this design could yield a nearly uniform vertical efficiency distribution [1].

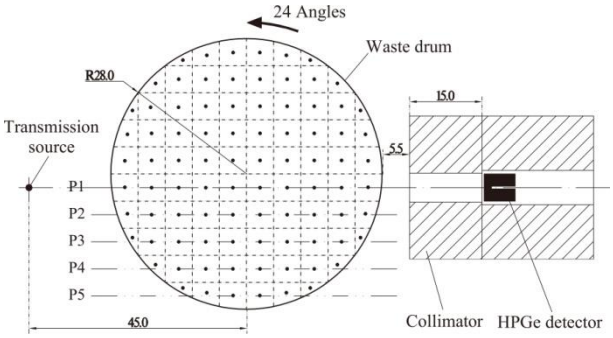

Fig.1 Vertical view of the TGS model (unit: **cm**).

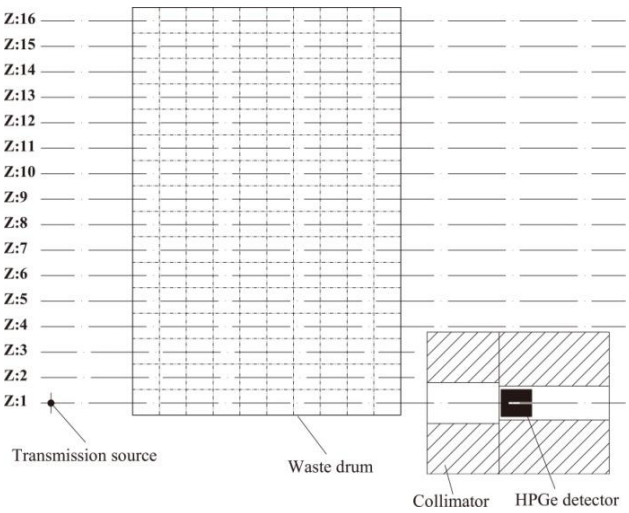

Fig.2 Side view of the TGS model.

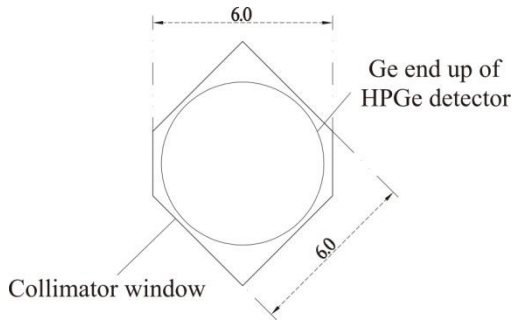

Fig.3 End cap and collimated window of the HPGe detector (unit: **cm**).

The scanning mode of the TGS instrument is stepwise with 5 translation positions along 1/10, 3/10, 5/10, 7/10, 9/10 of the drum radius displayed in Fig. 1 marked P1, P2, P3, P4 and P5, respectively. There are 24 successive rotation positions uniformly over 360° in each translation position. Each layer should be measured according to the elevation sequence number displayed in Fig. 2, which means that the number of TGS measurement geometries of the whole drum for transmission and emission reconstruction stages are 16*5*24 = 1,920, respectively.

2.1 Emission reconstruction equations

If there is absence of attenuation matrices in the waste drum, the measured gamma radio-activity can be characterized as follows:

$$\mathbf{D} = \mathbf{E} \bullet \mathbf{S} \tag{1}$$

or

$$D_i = \sum_{j}^{JJ} E_{ij} \bullet S_j \tag{2}$$

where $\mathbf{D}$, $\mathbf{E}$ and $\mathbf{S}$ are the count rate matrix, the detection efficiency matrix and the radio-activities matrix of point sources respectively; D_i is the count rate of the ith measurement position, which all come from inner-drum gamma sources contribution without any attenuation; E_{ij} is the detection efficiency of the jth voxel at the ith measurement position; JJ is the total number of voxels in waste drum; S_j is the radio-activity of gamma source in the jth voxel.

If there are attenuation materials in the nuclear waste drum, the attenuation condition must be taken into account to modify the detection efficiency matrix in the Eqs. (1) and (2) to attenuation- -corrected emission reconstruction equations as follows:

$$\mathbf{D} = \mathbf{F} \bullet \mathbf{S} = \left(\mathbf{E} \bullet \mathbf{A}\right) \bullet \mathbf{S} \tag{3}$$

or

$$D_i = \sum_{j}^{JJ} F_{ij} \bullet S_j = \sum_{j}^{JJ} \left(E_{ij} \bullet A_{ij}\right) \bullet S_j \tag{4}$$

where $\mathbf{F}$ is the attenuation-corrected detection efficiency matrix considering the loss of photons due to attenuation materials inside the drum; $\mathbf{A}$ is the attenuation-corrected factors matrix obtained by emission-computed path lengths combined with transmission-reconstructed linear attenuation coefficients of all voxels inside the drum using a gamma transmission source outside the drum displayed in Fig. 1; A_{ij} is the attenuation-corrected factor of photons emitted from the jth voxel in the ith emission measurement. A_{ij} can be estimated using Beer's Law as follows[6]:

$$A_{ij} = \prod_{k} \exp\left(-\mu_k x_{ijk}\right) \tag{5}$$

where x_{ijk} is the path length in the kth voxel along the path that gamma rays emit from the jth voxel to the HPGe detector at the ith emission measurement. Therefore, the emission reconstruction issue is transformed to find the solutions of the attenuation-corrected linear equations shown in equation (3). Thus, the total gamma radio-activity is found by summing the individual S_j over the whole drum.

As a result, the size of the huge detection efficiency matrix is 1,408*1,920 = 2,703,360, which means that the same number of detection efficiency matrix elements must have to be calibrated. If conventional physical experiment methods and routine theoretical calculations of using Monte Carlo methods are applied, the detection efficiency calibration workload will be extraordinary enormous, time-consuming and difficult to implement. Therefore, TGS measurement geometries are analyzed in detail from three aspects, *i.e.*, limited fields of view (FOVs) of the collimated High Purity Germanium (HPGe) detector, the spatial position overlap and symmetry of point sources relative to the collimated HPGe detector, intending to obtain independent matrix elements in calibrated detection efficiency matrix to avoid redundant workload.

2.2 Limited FOVs of the collimated HPGe detector

When considering relevant FOVs, the HPGe-detector end cap and its collimator must have to be taken into consideration seriously and discreetly because it is just them that have the full authority of the FOVs of the collimated HPGe detector. FOVs of the collimated HPGe detector have been carefully and accurately calculated theoretically depending on all 1,920 TGS measurement geometrical models to judge whether all the 1,408 point sources are within corresponding FOVs of the collimated HPGe detector for all translation, rotation and elevation positions. If the position of a point source is in the current FOV, corresponding Monte Carlo simulation of this point source without any attenuation should be conducted to obtain its detection efficiency. According to the

current TGS configuration displayed in Figs. 1 and 2, FOVs show that voxels in 13 layers at most can be detected by the collimated HPGe detector, *i.e.*, the layer where HPGe detector located and 6 layers each on both sides. When HPGe detector is at the bottom layer or the top layer, only 7 layers are in the FOVs at most. In each detected layer, not all point sources are in FOVs and make contributions to the counts of HPGe detector.

2.3 Position symmetry of point sources relative to the collimated HPGe detector

Provided that the HPGe detector and its collimator have the same symmetric axis displayed in Fig. 3, if the spatial positions of different point sources inside the drum are spatially symmetric to this symmetric axis, their detection efficiencies must be equal. Among 13 layers in FOVs of the collimated HPGe detector, the upper and lower 6 layer on both sides of the layer HPGe detector located are symmetrical, which means that only detection efficiencies of point sources of 7 layers on one side have to be calibrated. At P1, P2 and P3 translation positions displayed in Fig. 1, point sources in regular voxels at these different 7 layers in FOVs are obviously bilateral symmetrical to the same symmetrical axis of the HPGe detector and its collimator when rotation angles are corresponding to 0°, 90°, 180°, and 270° respectively.

2.4 Position overlap of point sources relative to the collimated HPGe detector

For rotation position overlap, spatial positions of point sources for all 6 rotation angles that cover 90° range totally overlap with point sources for the other 18 rotation angels. Note that for translation overlap, translation position overlap is too notable at the first rotation angle 0° to neglect a sharp decline in the number of point sources positions which are needed to be calibrated in voxels of the same regular shape compared to the other 5 rotation angles. Besides, for elevation overlap of 16 layers displayed in Fig. 2, spatial positions of point sources in FOVs when measuring one layer will totally overlap with that of the next layer to be measured. Therefore, only one layer needs to be measured when carrying out the calibration of detection efficiency but not 16 layers because of elevation position overlap.

When measuring the first layer labeled "**Z:1**" at the first rotation angle 0° and the P1 translation position displayed in Figs. 1 and 2, spatial positions of point sources inside the drum whose corresponding detection efficiencies must have to be computed are displayed in Fig. 4 when considering limited FOVs of the collimated HPGe detector, position symmetry and overlap of point sources relative to collimated HPGe detector.

As a result, numbers of independent detection efficiency matrix elements are displayed in Table 1, which are corresponding to spatial positions of point sources in 6 rotation angles over 90° rotation angle range at all 5 translation and 16 elevation positions. Therefore, there are 175+411+389+405+405+402 = 2,187 independent detection efficiency matrix elements, which only account for about 0.08% of the original 2,703,360 detection efficiency elements needed to be calibrated, meaning that detection efficiency calibration workload are greatly reduced according to the TGS configuration used in this paper.

Table 1 Numbers of independent detection efficiency matrix elements of 6 rotation angles over 90° rotation angle range at all translation and elevation positions

rotation angles	0°	15°	30°	45°	60°	75°
numbers of independent matrix elements	175	411	389	405	405	402

3 Simulation verification of detection efficiency calibration

To verify the 3D detection efficiency calibration results, two 200 liters drums are established with different kinds of attenuation matrices but with the same distribution of three ^{60}Co point sources with distinct radioactive levels at different radial and axial positions displayed in Fig. 5. These 3 point sources are located in the center of their own corresponding voxels. In MCNP simulations, only counts from the 1.3325 MeV ^{60}Co gamma rays are obtained by the collimated HPGe detector without considering the counting time. The standard counts of these point sources A, B and C simulated in Monte Carlo simulations are $3.0*10^8$, $2.0*10^8$ and $5.0*10^8$, respectively.

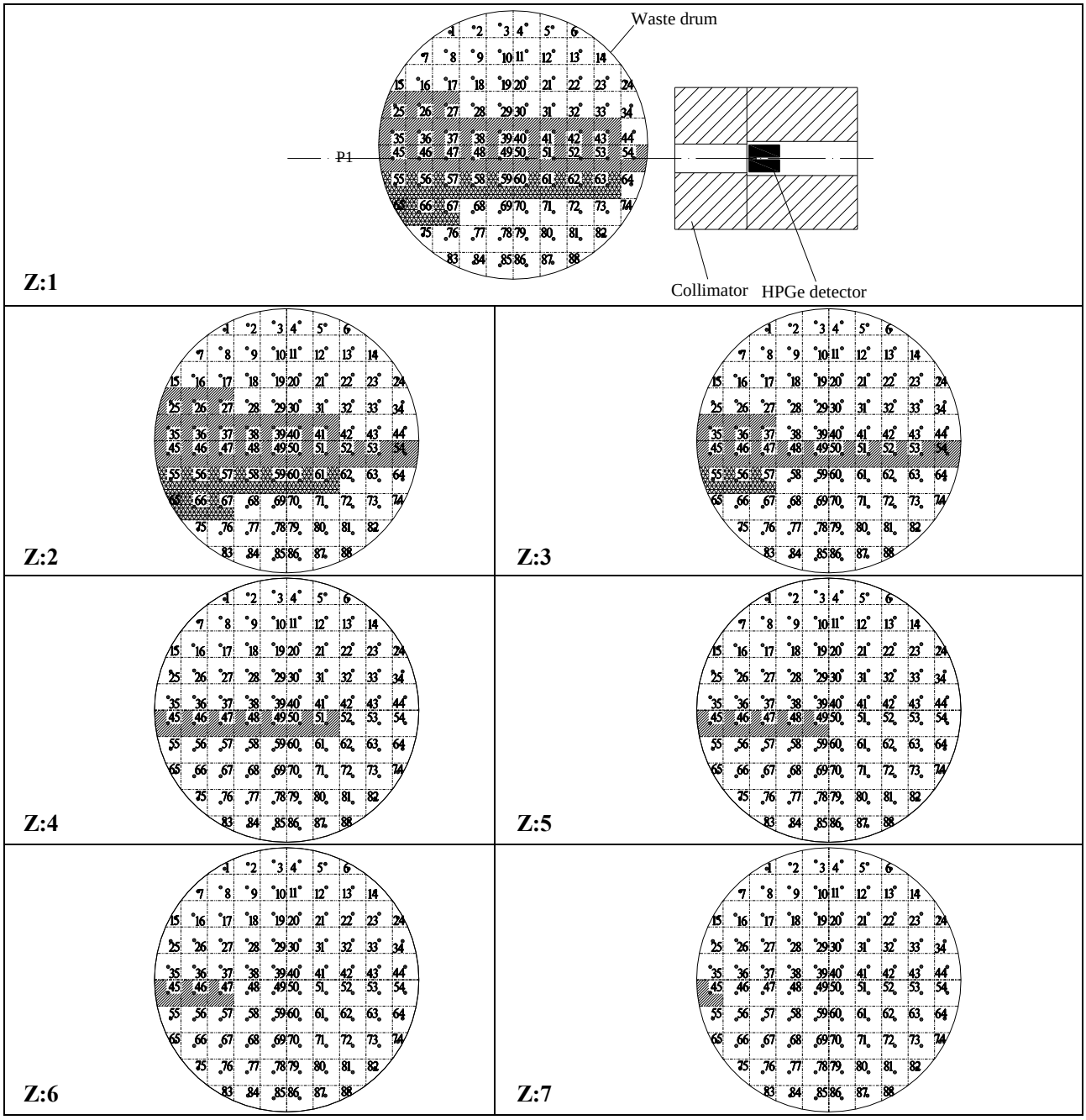

Fig.4 Point sources in FOVs at the first rotation angle 0° when emission-measuring the first layer at the P1 translation position.

(Point sources in voxels with ○ and ◍ shadow are in FOVs, but detection efficiencies of the former must be calibrated but the latter not because of the position symmetry of point sources.)

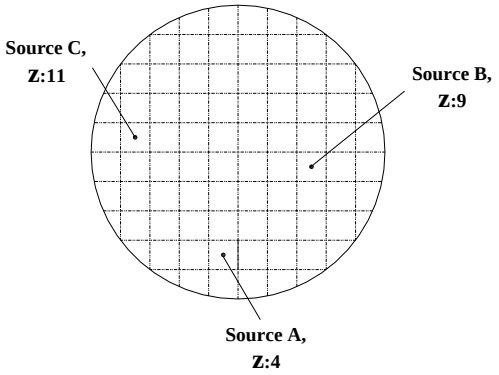

Fig.5 Distribution of 3 point sources in drums.

The first drum is fully filled with air whose linear attenuation coefficient is thought to be zero, and there is no attenuation matrix inside the drum. The second drum is fully filled with uniform and homogeneous wood with density of 0.433 g/cm^3 and the ideal linear attenuation coefficient of 0.02518 cm^{-1} at 1.3325 MeV, which is computed by an extra MCNP simulation. In order to get rid of the influence of transmission reconstruction, each voxel in the second drum is thought with this ideal linear attenuation coefficient.

Average emission path lengths of 1,408 point sources at 1,920 measurement positions in FOVs of the collimated HPGe detector can be obtained by considering the irregular edge shape of the real drum[5] combined with applied the "point-detector (PD)" model, which divides the end cap of HPGe detector into 10*10 parts and only take advantage of 80 parts inside the end cap of HPGe detector[7]. When using the "point-detector (PD)" model in the emission reconstruction stage, the "point" is corresponding to each point source in the drum instead of the transmission source in the transmission reconstruction stage and the "detector" is still corresponding to the actual collimated HPGe detector. Based on the ideal linear attenuation coefficient and the computed average emission path lengths, the influence of attenuation matrices inside the drum on the emission reconstruction radio-activities will be eliminated to the utmost extent in the second drum. Both of Algebraic Reconstruction Technique (ART) with the non-negativity constraint and Maximum Likelihood Expectation Maximization (MLEM) are used as the emission reconstruction algorithms when assaying these two kinds of waste drums.

4 Results and discussion

4.1 Emission-reconstructed results of the first air drum

Emission-reconstructed results of the air drum are displayed in Table 2 and the so-called "summed" results are corresponding to the total counts of each distinct point source by summing all counts in the neighboring voxels. It can be seen that the summed results are clearly better than those that directly come from emission-reconstructed values and are not summed. Emission reconstruction images of 16 layers in air drum using ART are displayed in Fig. 6, respectively. Emission-reconstructed images of air drum using MLEM are similar to Fig. 6 and will not be displayed.

4.2 Emission-reconstructed results of the second wood drum

Emission-reconstructed results of the wood drum are displayed in Table 3. It can be seen that the summed results are also better than those that are not summed. Emission reconstruction images of 16 layers using ART and MLEM are also similar to Fig. 6 and will not be displayed.

Table 2 Emission-reconstructed counts and relative errors of 3 point sources in the air drum

	ART		ART (Summed)		MLEM		MLEM (Summed)	
	Counts ($*10^8$)	Relative error (%)	Counts ($*10^8$)	Relative error (%)	Counts ($*10^8$)	Relative error (%)	Counts ($*10^8$)	Relative error (%)
point source A	2.97788	-0.73730	2.98611	-0.46313	2.97946	-0.68470	2.98419	-0.52693
point source B	1.98048	-0.97620	1.98301	-0.84950	1.97928	-1.03610	1.98168	-0.91590
point source C	4.96062	-0.78764	4.97579	-0.48412	4.95357	-0.92858	4.95541	-0.89182

Table 3 Emission-reconstructed counts and relative errors of 3 point sources in the wood drum

	ART		ART (Summed)		MLEM		MLEM (Summed)	
	Counts ($*10^8$)	Relative error (%)	Counts ($*10^8$)	Relative error (%)	Counts ($*10^8$)	Relative error (%)	Counts ($*10^8$)	Relative error (%)
point source A	2.97487	-0.83752	2.97904	-0.69880	2.94684	-1.77213	2.97662	-0.77931
point source B	1.96116	-1.94175	1.96639	-1.68069	1.94733	-2.63353	1.96894	-1.55287
point source C	4.96066	-0.78687	4.97000	-0.60010	4.90112	-1.97762	4.96135	-0.77299

From results mentioned above, all 3 point sources in both drums which contain attenuation matrices or not can be accurately located with different radioactive levels using ART or MLEM algorithms. Emission- -reconstructed relative errors of 3 point source in both drums are around 3% within the ideal [-20%, +20%] relative error range, which verifies the accuracy of non-attenuated 3D detection efficiency calibration results to prove the feasibility of the point source model used to simply calibrate detection efficiency in the TGS technique.

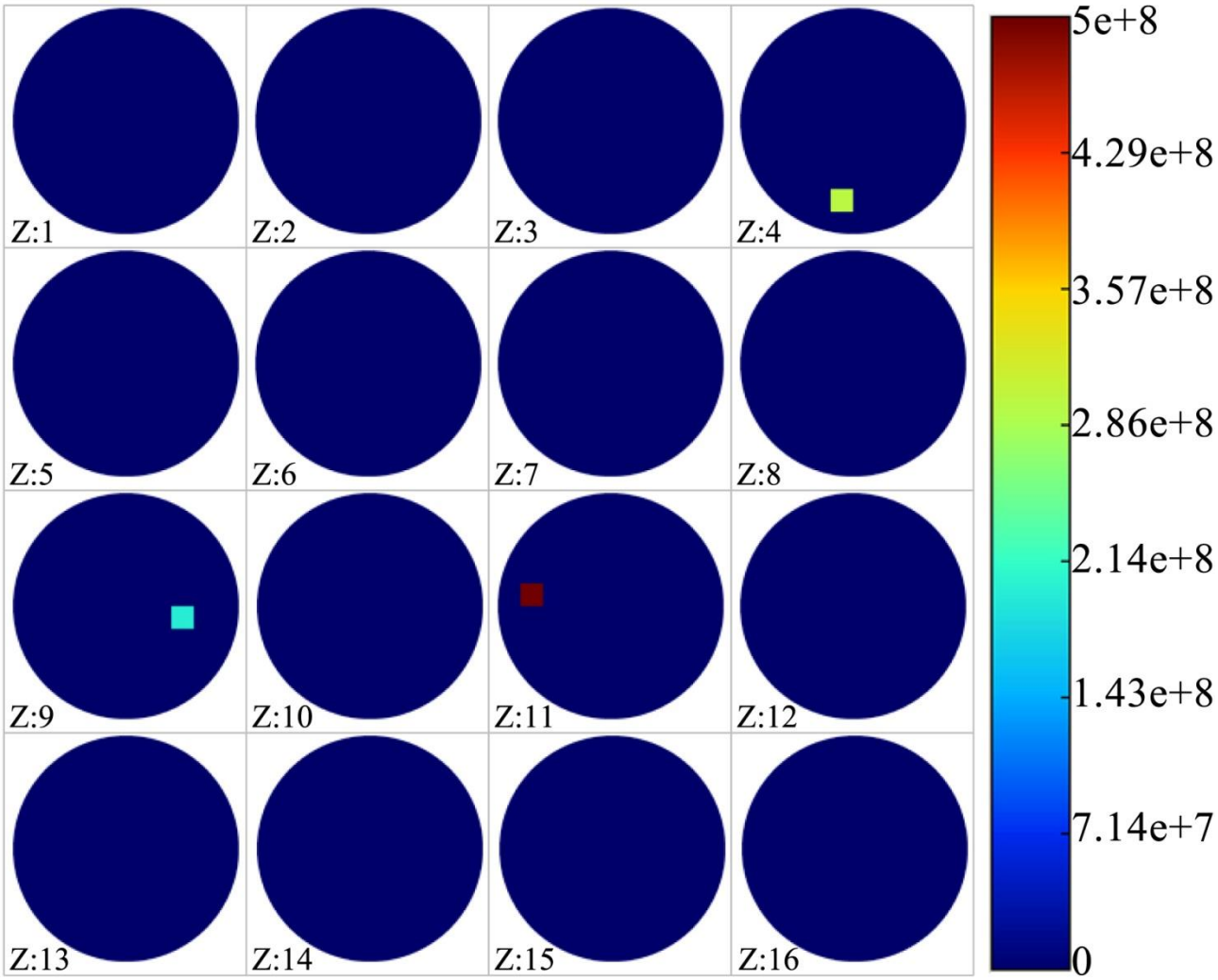

Fig.6 Emission-reconstructed images displaying the distribution of three point sources.

5 Conclusion

In this paper, a simplified detection efficiency calibration method using the point source model is proposed in Tomographic Gamma Scanning (TGS) technique. In a series of different measurement positions, TGS configurations are carefully analyzed to exploit limited field of views (FOVs) of the collimated HPGe detector, the position overlap and symmetry of point sources relative to the collimated HPGe detector in order to eliminate redundant workload of 3D detection efficiency calibration. Results show that only about 0.08% of the original workload is needed to be done according to the method used in this paper. In order to verify the effectiveness of obtained 3D detection efficiency distribution results, two different 200 liters waste drums are built up with the same distribution of 3 point sources with different positions and radioactive levels. Emission-reconstructed results using ART and MLEM algorithms reveal that different point sources can be easily and accurately located and their emission-reconstructed counts match with standard setting values very well with relative errors around 3%, which verifies and validates the effectiveness and feasibility of the method introduced in this paper. Thus, the method is valid and can be further extended to a wider range of application for various types of detectors to assay waste drums using Tomographic Gamma Scanning technique.

References

[1] ESTEP Robert J.: A preliminary design study for improving performance in tomographic assays, LA-12727-MA, Los Alamos National Lab., 1994.

[2] VENKATARAMAN, R., BRONSON, F., and ALRASHKEVICH, V., *et al.*: Validation of in situ object counting system (ISOCS) mathematical efficiency calibration software, Nuclear Instruments and Methods in

Physics Research Section A: Accelerators, Spectrometers, Detectors and Associated Instrument, 1999, 442: 450-454.

[3] MENAA, N., NAKAZAWA, D., and YANG, H., *et al.*: An Integrated Waste Assay System Using Tomographic and Segmented Gamma Scanning for Nuclear Power Plant Applications, Proceeding of Waste Management WM'10 Conference, Arizona, USA, 2010.

[4] BRIESMEISTER Judith F.: MCNP – A general Monte Carlo N-Particle transport code, LA-12635-M, Los Alamos National Labortary, 1997.

[5] HAN Miaomiao, GUO Zhirong, and LIU Haifeng, *et al.*: Novel edge treatment method for improving the transmission reconstruction quality in Tomographic Gamma Scanning, Applied Radiation and Isotopes, 2018, 135: 232-238.

[6] INTERNATIONAL ATOMIC ENERGY AGENCEY: Industrial Process Gamma Tomography: Final report of a coordinated research project 2003-2007, 2008.

[7] HAN Miaomiao, GUO Zhirong, and LIU Haifeng, *et al*.: Influence of different path length computation models and iterative reconstruction algorithms on the quality of transmission reconstruction in Tomographic Gamma Scanning, Nuclear Instruments and Methods in Physics Research Section A: Accelerators, Spectrometers, Detectors and Associated Instrument, 2017, 861: 16-22.